1 **Binding of Intercellular Adhesion Molecule 1 to β_2-Integrin Regulates Distinct**

2 **Cell Adhesion on Hepatic and Cerebral Endothelium**

3

4 Chun-Fang Tong[1], Yan Zhang[1,2], Shou-Qin Lü[1,2], Ning Li[1], Yi-Xin Gong[1], Hao Yang[1],

5 Shi-Liang Feng[1], Yu Du[1], Dan-Dan Huang[1], and Mian Long[1,2,]

6

7 [1]Center of Biomechanics and Bioengineering, Key Laboratory of Microgravity

8 (National Microgravity Laboratory), and Beijing Key Laboratory of Engineered

9 Construction and Mechanobiology, Institute of Mechanics, Chinese Academy of

10 Sciences, Beijing, China

11 [2]School of Engineering Science, University of Chinese Academy of Sciences, Beijing

12 100049, China.

13

14 **Running title:** Biophysical regulation of hepatic and brain ICAM-1s

15

16 **Key words:** Liver, brain, integrin, ICAM-1, kinetics

17

18 **Correspondence:**

19 Dr. Mian Long, Institute of Mechanics, Chinese Academy of Sciences, China. Tel:

20 +86-10-82514131. Fax: +86-10-82514131. E-mail: mlong@imech.ac.cn.

21

Downloaded from www.physiology.org/journal/ajpcell by ${individualUser.givenNames} ${individualUser.surname} (163.015.154.053) on August 28, 2018.
Copyright © 2018 American Physiological Society. All rights reserved.

22 ## Abbreviations

23

2D	two-dimensional
3D	three-dimensional
BBB	Blood brain barrier
BMEC	cerebral microvascular endothelial cells
bEnd.3	cerebral endothelial cell line
BM	bone marrow
FEM	finite element method
FITC	fluorescein isothiocyanate
hRBCs	human red blood cells
ICAM-1	intercellular adhesion molecule-1
LFA-1	lymphocyte function-associated antigen-1
LSEC	liver sinusoidal endothelial cell
Mac-1	macrophage-1 antigen
MAT	micropipette aspiration technique
MCM	Monte-Carlo method
PMN	neutrophil

24

Downloaded from www.physiology.org/journal/ajpcell by ${individualUser.givenNames} ${individualUser.surname} (163.015.154.053) on August 28, 2018.
Copyright © 2018 American Physiological Society. All rights reserved.

25 ## Abstract

26

27 Flowing neutrophils (PMNs) are forced to recruit towards inflamed tissue and adhere
28 on vascular endothelial cells, which is primarily mediated by the binding of
29 β_2-integrins to ICAM-1s. This process is distinct among different organs such as liver
30 and brain, however, the underlying kinetic and mechanical mechanisms regulating
31 tissue-specific recruitment of PMNs remain unclear. Here binding kinetics
32 measurement showed that, ICAM-1 on murine hepatic sinusoidal endothelial cells
33 (LSECs) bound to lymphocyte function-associated antigen-1 (LFA-1) with higher on-
34 and off-rates but lower effective affinity compared to macrophage-1 antigen (Mac-1),
35 while ICAM-1 on cerebral endothelial cells (BMECs or bEnd.3 cells) bound to LFA-1
36 with higher on-rates, similar off-rates and higher effective affinity compared with
37 Mac-1. Physiologically, free crawling tests of PMN onto LSEC, BMEC or bEnd.3
38 monolayer were consistent with those kinetics differences between two β_2-integrins
39 interacting with hepatic sinusoid or cerebral endothelium. Numerical calculations and
40 Monte Carlo simulations validated tissue specific contributions of
41 β_2-integrin-ICAM-1 kinetics to PMN crawling on hepatic sinusoid or cerebral
42 endothelium. Thus, this work first quantified the biophysical regulation of PMN
43 adhesion in hepatic sinusoids compared with cerebral endothelium.

44

Downloaded from www.physiology.org/journal/ajpcell by ${individualUser.givenNames} ${individualUser.surname} (163.015.154.053) on August 28, 2018.
Copyright © 2018 American Physiological Society. All rights reserved.

45 # Introductions

46

47 Neutrophil (PMN) recruitment and transmigration through endothelium is crucial in
48 inflammatory responses for host defense against infection and wound healing (10, 40).
49 These processes occur virtually in all the organs such as liver or brain, but the
50 molecular mechanisms mediating PMN recruitment are not exactly the same among
51 distinct organs (33). For example, selectin-dependent PMN rolling is critical for their
52 recruitment to mesenteric, cremasteric postcapillary venules, or cerebral endothelium,
53 but not for their incidence in hepatic sinusoid (30). Moreover, cellular adhesive
54 molecules acting in PMN adhesion and crawling are distinct for both hepatic
55 sinusoids and cerebral endothelium (33). While β_2-integrin and its ICAM-1 ligand are
56 known to play important roles in these processes (18, 30, 33), the mechanisms how
57 these receptor-ligand interactions regulate tissue-specific PMN recruitment remain
58 unclear yet.

59

60 Hepatic microcirculation is specific due to its complicated, three-dimensional (3D)
61 microenvironment of sinusoidal nodes. Peripheral PMNs are forced by blood flow to
62 interact with resident Kupffer cells and hepatic sinusoidal endothelial cells (LSECs)
63 and initiate hepatic inflammatory cascades *via* cytokine production. Thus,
64 understanding the adhesion between these cells is critical for PMN recruitment and
65 immune responses in hepatic sinusoids (4, 23). Macrophage-1 antigen (Mac-1), one of
66 β_2-integrin members, is assumed to play a key role in hepatic immune responses

Downloaded from www.physiology.org/journal/ajpcell by ${individualUser.givenNames} ${individualUser.surname} (163.015.154.053) on August 28, 2018.
Copyright © 2018 American Physiological Society. All rights reserved.

67 because this molecule dominates PMN adhesion and crawling in the presence of
68 localized fMLF-induced stimuli in the sinusoids (30). Activated lymphocyte
69 function-associated antigen-1 (LFA-1) also enable PMNs to firmly adhere to the
70 sinusoidal endothelium and to further extravasate into the liver parenchyma in the
71 presence of chemokines (34). Intriguingly, the role of LFA-1 in liver function remains
72 controversial compared to that for Mac-1.
73
74 Brain has a unique blood brain barrier (BBB) structure composed of endothelial cells
75 with tight junction, integrated basement membrane, pericytes and astrocytes, which
76 could block nearly all polar or large compounds (5, 39). Cerebral microvascular
77 endothelial cells (BMECs) interact with PMNs through adhesive molecules such as
78 ICAM-1 and VCAM-1 (2). On the BBB, LFA-1 plays more important role in
79 mediating PMN shear-resistant arrest while Mac-1 is dominant in mediating PMN
80 polarization (18). Evidently, the same molecular pair of β_2-integrin-ICAM-1 binding
81 presents distinct roles when PMNs are forced to recruit onto hepatic or cerebral
82 endothelium.
83
84 Cell adhesion and crawling are governed by their binding kinetics of interacting
85 receptor-ligand pairs. In contrast to 3D binding kinetics in bulk chemistry, where at
86 least one molecular species is in solution, the determination of two-dimensional (2D)
87 kinetics for surface-bound molecules requires distinct biophysical approaches (15).
88 One well-defined approach is an adhesion frequency assay, extensively applied to

Downloaded from www.physiology.org/journal/ajpcell by ${individualUser.givenNames} ${individualUser.surname} (163.015.154.053) on August 28, 2018.
Copyright © 2018 American Physiological Society. All rights reserved.

89 quantify the binding kinetics of selectin- and integrin-ligand interactions on two
90 opposed cell surfaces (16, 19, 20, 43, 44). Meanwhile, *in vitro* functional assays are
91 preferential for validating the kinetic regulation of cell adhesion and crawling
92 mediated by cellular adhesive molecules (31 37, 41). Combining these approaches, we
93 quantified here the kinetics differences underlying the adhesion of ICAM-1s from
94 hepatic sinusoidal endothelial cells (LSECs) or cerebral microvascular endothelial
95 cells (BMECs and bEnd.3 cells) to their partners, LFA-1 and Mac-1. The free
96 dynamics of PMN crawling onto LSEC, BMEC or bEnd.3 monolayer were also
97 measured experimentally and discussed with numerical calculations.
98

Downloaded from www.physiology.org/journal/ajpcell by ${individualUser.givenNames} ${individualUser.surname} (163.015.154.053) on August 28, 2018.
Copyright © 2018 American Physiological Society. All rights reserved.

99 # Materials and Methods

100

101 ## Ethics statement

102 All experiments involving the use of human blood and live animals were conducted in
103 accordance with the guidelines of the Institutional Animal and Medicine Ethical
104 Committee (IAMEC), and all the protocols were approved by the IAMEC at the
105 Institute of Mechanics, Chinese Academy of Sciences. Whole human blood was
106 obtained from randomly selected, healthy human donors after informed consent was
107 signed.

108

109 ## Reagents

110 Recombinant mouse LFA-1 (CD11aCD18) or Mac-1 (CD11bCD18) constructs and
111 ICAM-1-Fc chimeras were from R&D (Minneapolis, USA). Rat anti-mouse
112 monoclonal antibodies (mAbs) against LFA-1 (M17/4) and Mac-1 (M1/70),
113 fluorescein isothiocyanate (FITC)-conjugated mAbs against LFA-1 (M17/4, 5.4
114 equivalent of FITC per molecule (F/P); 2D7, F/P = 4.6), Mac-1 (M1/70, F/P = 6.4),
115 and ICAM-1 (CD54; YN1/1.7.4, F/P = 5.9), as well as APC-conjugated Ly-6G/Ly-6C
116 (Gr-1) (RB6-8C5), PerCP/Cy5.5-conjugated anti-F4/80 (BM8), and FITC-conjugated
117 anti-CD146 mAbs (ME-9F1) were from Biolegend (San Diego, USA). Rat anti-CD31
118 (MEC 7.46) and goat anti-rat IgG H&L (Alexa fluor 488) antibodies were from
119 Abcam (Shanghai, China). Collagenase IV (C5138), Percoll (P1644),
120 lipopolysaccharide (LPS; L2800) and DNAse (D4513) (used for primary BMEC

Downloaded from www.physiology.org/journal/ajpcell by ${individualUser.givenNames} ${individualUser.surname} (163.015.154.053) on August 28, 2018.
Copyright © 2018 American Physiological Society. All rights reserved.

121 isolation) were from Sigma-Aldrich (St. Louis, USA). Rat tail collage I was from
122 Corning (New York, USA). bFGF (100-18B) was from Peprotech (New Jersey, USA).
123 Mouse recombinant TNF-α (410-MT-010) was from R&D (Minneapolis, USA), and
124 bovine serum albumin (BSA; BSAS-AU) was from Bovogen (Melbourne, Australia).
125 Pyrumycin (A1113802) and fibronectin (33016015) were from Thermo Fisher
126 (Waltham, MA). Optiprep™ was from Axis-shield (Scotland). Collagenase-dispase
127 (10269638001) and DNAse (11284932001) (used for primary LSEC isolation) were
128 from Roche (Basel, Switzerland). Collagenase CLS2 (LS004176) was from
129 Worthington (Ohio, USA). Endothelial Cell Medium (ScienCell 1001) were from
130 Sciencell (San Diego, USA).
131
132 **Cells**
133 bEnd.3 cells from American Type Culture Collection were cultured in Endothelial
134 Cell Medium with 5% FBS, 100 U/ml penicillin, 100 mg/ml streptomycin and 1%
135 100× ECGS (Endothelial Cell Growth Supplement). Mouse LSECs, BMECs and bone
136 marrow (BM)-derived PMNs were isolated from 8-12-week-old male C57BL/6 mice
137 (Vital River Laboratories, Beijing, China) as described below. The sorted LSECs were
138 cultured in high glucose DMEM supplemented with 10% FBS, 100 U/ml penicillin,
139 10 mg/ml streptomycin and 1 mM L-glutamine at 37°C with 5% CO_2. Isolated
140 BMECs were cultured in high glucose DMEM supplemented with 20% FBS, 10 μg/L
141 bFGF, 20 mg/ml heparin, 1 mg/ml 100 U/ml penicillin, 10 mg/ml streptomycin and 1
142 mM L-glutamine on a dish pre-coated by 200 μg/ml collagen I and 10 μg/ml

Downloaded from www.physiology.org/journal/ajpcell by ${individualUser.givenNames} ${individualUser.surname} (163.015.154.053) on August 28, 2018.
Copyright © 2018 American Physiological Society. All rights reserved.

143 fibronectin after two-day pre-culture in the medium with additional 2 mg/L
144 pyrumycin for cell purifying. In chemokine or chemoattractant stimulation tests,
145 LSECs, MBECs or bEnd.3 cells were cultured for 24 h in the medium before being
146 incubated with LPS or TNF-α for additional 12 h. In blocking cases, BM PMNs were
147 co-cultured with anti-LFA-1 or anti-Mac-1 mAbs in DPBS for 45 min at 4°C before
148 use.

149

150 **Isolation of LSECs**

151 Mouse LSECs were isolated from the liver of anesthetized 8-12-week-old male
152 C57BL/6 mice. The liver was perfused *via* the portal vein at 5 ml/min for 5 min with a
153 balanced salt solution containing 5 mM glucose, 0.01% sodium heparin, and 5 mM
154 EGTA, followed by 25 ml of 4 mM $CaCl_2$, 0.5% BSA, 2% FBS and 0.05%
155 collagenase IV in high glucose DMEM at 5 ml/min. The isolated liver was minced,
156 stirred in 10 ml of high glucose DMEM supplemented with 0.014 mg/ml DNAse, 4.3
157 mM $MgCl_2$, 0.05% BSA, and 2% FBS at 37°C at pH 7.4 for 10 min, and then washed
158 twice in 50 ml of DMEM with 2% FBS at 54×g for 3 min to remove tissue sediments.
159 Collected supernatant was centrifuged at 500×g for 8 min, and the sediments were
160 re-suspended for density gradient equilibrium centrifugation at 1400×g for 18 min at
161 4°C. Mouse non-parenchymal cells containing LSECs and other non-hepatocyte cells
162 were finally collected from the layer between 11% and 17.6% in an Optiprep^{TM}
163 density gradient, re-suspended in 14 ml of staining buffer solution, centrifuged at
164 500×g for 10 min, and then stained with anti-CD146 and anti-F4/80 mAbs in 100 μl

Downloaded from www.physiology.org/journal/ajpcell by ${individualUser.givenNames} ${individualUser.surname} (163.015.154.053) on August 28, 2018.
Copyright © 2018 American Physiological Society. All rights reserved.

165 of staining buffer solution for 45 min. Cell sorting was conducted to isolate LSECs at
166 a purity of 95.6-99.0%.
167
168 **Isolation of BMECs**
169 BMECs were isolated from 8-10 adult C57BL/6 mice (8-12-week-old male) sacrificed
170 by cervical dislocation (35). After removing brain stems, cerebella, thalami, outer
171 vessels and meninges from the brains, the preparations were pooled and homogenized
172 in 13.5 ml high glucose DMEM solution and first digested with 6 mg collagenase
173 CLS2 and 0.2 mg DNAse for 1 h at 180 rpm at 37°C. The digestion was stopped by
174 10 ml high glucose DMEM solution and centrifuged at 1000×g for 10 min at 4°C. The
175 myelin was then removed with 20% BSA in 25 ml high glucose DMEM solution at
176 1,000×g for 20 min at 4°C. The pellet was re-suspended with 2 ml high glucose
177 DMEM solution containing 1 mg/ml collagenase/dispase and 0.2 mg DNAse and
178 digested for 1 h at 180 rpm at 37°C. During the second digestion, the suspension was
179 centrifuged in Percoll solution (10 ml Percoll with 19 ml 1× PBS, 1 ml 10× PBS and 1
180 ml FBS) to set up the density gradient at 2,700×g for 1 h at 4 °C, with acceleration,
181 without brake. After washing with 10 ml high glucose DMEM solution, 2 ml DMEM
182 resuspension was added to the Percoll gradient and centrifuged at 700×g for 10 min at
183 4°C without acceleration and brake. Collected 12 ml suspension around the interface
184 was centrifuged in 50 ml DMEM at 1000×g for 10 min at 4°C. Packed cells were first
185 cultured in medium with 2 mg/L pyrumycin for two days and then switched to the
186 conventional culture medium. Cells after one split were used for functional

Downloaded from www.physiology.org/journal/ajpcell by ${individualUser.givenNames} ${individualUser.surname} (163.015.154.053) on August 28, 2018.
Copyright © 2018 American Physiological Society. All rights reserved.

187 experiments. Cell sorting was conducted to isolate BMECs at a purity around 99.0%
188 and the sorted cells were identified by immunofluorescence staining for the
189 endothelial cell marker CD31 (*data not shown*).
190

191 **Isolation of BM PMNs**

192 BM PMNs were also isolated from 8-12-week-old male C57BL/6 mice sacrificed by
193 cervical dislocation. The cell suspensions harvested from the BM of the femur and
194 tibia were centrifuged at 300 rpm for 10 min and then re-suspended in DPBS
195 supplemented with 0.5% BSA and 2 mM EDTA for an equilibrium centrifugation
196 using a Ficoll-Hypaque density gradient (Histopaque-1077 and Histopaque-1119;
197 Sigma-Aldrich). Enriched BM PMNs collected at the interface between the two layers
198 were washed twice and then kept in DPBS with 0.5% BSA for 45 min at 4°C before
199 use.
200

201 **Protein coating and site density determination**

202 Human red blood cells (hRBCs) isolated from fresh whole blood were used to serve
203 as the carriers for target molecule presentation and as the detector for cell adhesion
204 test. A chromium chloride protocol was used to covalently coat LFA-1, Mac-1, or
205 irrelevant goat-anti-human IgG polyclonal antibodies onto the hRBC surface (22, 28).
206 Coating efficiency was analyzed by flow cytometry (37).
207

208 Site densities of LFA-1s, Mac-1s on hRBC or PMNs and of ICAM-1s on endothelial

Downloaded from www.physiology.org/journal/ajpcell by ${individualUser.givenNames} ${individualUser.surname} (163.015.154.053) on August 28, 2018.
Copyright © 2018 American Physiological Society. All rights reserved.

209 cells were measured *via* flow cytometry. Cells were incubated with 10 μg/ml of
210 FITC-anti-LFA-1 or -Mac-1 or -ICAM-1 mAbs in DPBS buffer on ice for 45 min and
211 washed before cytometry analysis. Fluorescence intensities of the stained cells were
212 quantified using standard fluorescence calibration beads (Quantum 25, Bangs
213 Laboratories Inc., Fishers, USA) to determine the mean number of molecules of
214 equivalent soluble fluorochrome (MESF) per cell. The MESF value was divided by
215 the F/P value of FITC-labeled mAbs and the surface area of hRBC (6 μm in diameter),
216 and then converted into the site density of the target molecules (19).
217
218 **Micropipette aspiration technique**
219 Cell adhesion and the underlying binding kinetics of interacting molecules between a
220 hRBC bearing LFA-1s or Mac-1s and a LSEC, BMEC or bEnd.3 cell expressing
221 ICAM-1s were determined using a previously described micropipette aspiration
222 technique (MAT) (15, 19). Before tests, LSECs, BMECs or bEnd.3 cells were
223 trypsinized and washed twice with fresh medium, and then resuspended in the same
224 medium used in micropipette aspiration assay to recover the cells for 1 h by rocking at
225 100 rpm at 37°C (16). Briefly, a hRBC and a LSEC, BMEC or bEnd.3 cell were
226 aspirated by two micropipettes respectively and driven by micromanipulation in an
227 approach-contact-withdrawal cycle under a microscope. An adhesion event was
228 determined *via* hRBC membrane deflection during the withdrawal phase (19).
229 Collectively, the specific adhesion frequency, P_a, at a given contact duration, t, was
230 determined from 80-100 repeated tests. For each molecular pair examined, a P_a *vs.* t

Downloaded from www.physiology.org/journal/ajpcell by ${individualUser.givenNames} ${individualUser.surname} (163.015.154.053) on August 28, 2018.
Copyright © 2018 American Physiological Society. All rights reserved.

231 curve corresponding to the site densities of the receptor (m_r) and ligand (m_l) was
232 obtained from 18-33 cell pairs. Each curve was fitted by the following simple kinetic
233 model (9):

234 $$P_a = 1 - \exp\{-m_r m_l A_c K_a[1 - \exp(-k_r t)]\} \quad \text{Eq. 1}$$

235 to estimate the zero-force off-rate, k_r, and the effective binding affinity, A_cK_a, where
236 A_c is the contact area, which was kept constant in all experiments by controlling a
237 suitable approach distance with piezo micromanipulation to reach the same
238 compressive state of the hRBC in the repeated events or tests (19).

239

240 **Parallel plate crawling test**

241 PMN free crawling on LSEC, BMEC or bEnd.3 monolayer was tested. Here LSECs,
242 BMECs and bEnd.3 cells were cultured on a 20 μg/ml collagen I pre-coated 15-mm
243 glass dish (NEST, China) for 48 h and pre-treated with 100 ng/ml TNF-α for 12 h
244 before adding in BM PMNs. In some cases, PMNs were pre-incubated with
245 anti-LFA-1 mAbs or anti-Mac-1 mAbs. Cell crawling tests were performed on an
246 inverted DIC microscope (IX83, Olympus, Japan) using a 60×/NA 1.35 objective.
247 After adding 5×10^5 PMNs onto LSEC, BMEC or bEnd.3 monolayer, PMN movement
248 was tracked for 1 h by capturing images from four randomly preset fields at a 30-s
249 interval. Analysis of PMN crawling speed and fraction was conducted using Image J
250 (National Institutes of Health, Bethesda, USA) manual tracking plugin. For a single
251 PMN, the moving speed was calculated between two sequential frames and then
252 averaged for the data spinning from 30 to 60 min. A crawling PMN was defined for an

Downloaded from www.physiology.org/journal/ajpcell by ${individualUser.givenNames} ${individualUser.surname} (163.015.154.053) on August 28, 2018.
Copyright © 2018 American Physiological Society. All rights reserved.

253 averaged moving velocity of ≥ 3 μm/min, in which the velocity threshold was
254 independently pre-determined for ≥ 14 cells with visible pseudopodia or movement.
255 The mean crawling speed of PMN was averaged for 96-224 cells from at least 3-6
256 replicates in each case, and the mean crawling fraction was estimated as the
257 percentage of crawling PMNs in total PMNs.
258
259 **Mechanical model and numerical simulation**
260 To correlate molecular kinetic parameters to PMN crawling speed on endothelium, a
261 mechanical model was developed. Generally, a 2D circular cell with radius r_{m} is
262 placed on the substrate with well-defined stiffness, K_s (Fig. 6A). Cellular cytoskeleton
263 is discrete by N nodes connected by the edges according to the Delaunay triangulation.
264 Each edge that connects neighboring nodes i and j (which represent the focal
265 adhesions) consists of a Hookean spring (which denotes the stress fiber). A sliding
266 friction element accounting for viscous dissipation effect is associated with
267 cytoskeleton-fluid friction. The whole model was divided into two modules, named as
268 cell mechanics and focal adhesion dynamics, respectively.
269
270 *Cell mechanics module*
271 In model setting, there are three types of forces acting on each node i, that is, the
272 substrate frictional drag force, passive elastic force, and active force, to expound cell's
273 movement together:
274 $$\overrightarrow{F_i^{\mathrm{drag}}} + \overrightarrow{F_i^{\mathrm{int}}} = \overrightarrow{F_i^{\mathrm{act}}}. \quad \text{Eq. 2}$$

Downloaded from www.physiology.org/journal/ajpcell by ${individualUser.givenNames} ${individualUser.surname} (163.015.154.053) on August 28, 2018.
Copyright © 2018 American Physiological Society. All rights reserved.

275 $\overrightarrow{F_i^{\text{drag}}}$ represents the resistance to active force, and is composed by two parts:

276
$$\overrightarrow{F_i^{\text{drag}}} = \eta v_i + \sum_{q=1}^{N_i^{\text{b}}} \overrightarrow{r_q^i} K_{\text{tot}}. \qquad \text{Eq. 3}$$

277 Here ηv_i denotes the resistant force independent of the substrate stiffness, where

278 η is the drag coefficient, and v_i is the nodal velocity. The second term on the right

279 denotes the resistant force arisen from mechanical stretch of integrin-ligand bonds,

280 where K_{tot} is the effective spring constant, $\overrightarrow{r_q^i}$ is the displacement vector of each

281 bond q of *i-th* node, and N_i^b is the total number of integrin-ligand bonds. $\overrightarrow{F_i^{\text{int}}}$ in

282 Eq. 2 denotes the sum of elastic stress at node i with j=1,…G_i neighboring nodes

283 while $\overrightarrow{F_i^{\text{act}}}$ terms the active forces. The magnitude dependence of cell-generated

284 traction force at *i-th* frontal node on cell-substrate adhesion strength can be described

285 by Langmuir–Hill equation (11).

286

287 *Focal adhesion dynamics module*

288 Formation of a focal adhesion complex is described as a stochastic process due to the

289 intrinsic features of 2D binding kinetics (9, 26) between the integrins on the cell and

290 their ligands on the surface of extracellular matrix. The transformation of integrin

291 from an inactive (low or intermediate affinity) to an active (high affinity) state is

292 induced by force applied on it (13). Evolution of active integrins and corresponding

293 initial conditions are given by the following ordinary differential equation,

294
$$\frac{dA_i}{dt} = S_i - \gamma A_i, \qquad \text{Eq. 4.1}$$

295
$$A_i(0) = A_i^0, \qquad \text{Eq. 4.2}$$

Downloaded from www.physiology.org/journal/ajpcell by ${individualUser.givenNames} ${individualUser.surname} (163.015.154.053) on August 28, 2018.
Copyright © 2018 American Physiological Society. All rights reserved.

296 where A_i is the number of active integrins at *i-th* node, γ is the delay rate of active

297 integrins, and S_i is the source term and defined as follows,

298 $$S_i = \begin{cases} S_0 + \dfrac{N^{\mathrm{tot}} - N^{\mathrm{act}}(t)}{N^{\mathrm{tot}} - N^{\mathrm{ini}}} \delta\rho & \text{if } f_q^i \geq F_{\mathrm{r}} \\ S_0 & \text{if } f_q^i < F_{\mathrm{r}} \end{cases}, \qquad \text{Eq. 5}$$

299 where S_0 is the basal integrin activation rate, N^{tot} is the total number of integrins

300 on the cell (active plus inactive), N^{ini} is the initial number of active integrins

301 ($N^{\mathrm{ini}} = \sum_i^N A_i^0$), $N^{\mathrm{act}}(t)$ is the number of active integrins during time evolution

302 ($N^{\mathrm{act}}(t) = \sum_i^N A_i(t)$), and $\delta\rho$ is the maximum number of integrins added after each

303 reinforcement event. f_q^i and F_{r} are the stretch force on one bond and its threshold

304 force, respectively.

305

306 Numerical simulations were carried out upon a finite element method (FEM) and a

307 Monte-Carlo method (MCM). Briefly, FEM is implemented to solve the mechanical

308 equilibrium equation (Eq. 2). In MCM, the reversible binding and unbinding events

309 between integrins and ICAM-1s are assumed to occur stochastically. The two modules

310 become interlinked by both invoking the stretch force applied on each integrin-ligand

311 bond (Eq. 3). Initially, all receptor molecules are assumed to be unbound. Each

312 simulation lasts 12 min with a time-step size of 0.3 ms.

313

314 **Statistical analysis**

315 Student's *t*-test was performed, and *P* values were calculated using the two-tailed *t*-test

Downloaded from www.physiology.org/journal/ajpcell by ${individualUser.givenNames} ${individualUser.surname} (163.015.154.053) on August 28, 2018.
Copyright © 2018 American Physiological Society. All rights reserved.

316 for groups with equal variances.

Downloaded from www.physiology.org/journal/ajpcell by ${individualUser.givenNames} ${individualUser.surname} (163.015.154.053) on August 28, 2018.
Copyright © 2018 American Physiological Society. All rights reserved.

317 **Table 1. Kinetic parameters used for numerical calculations**

Parameter description	Symbol	Value	Sources
Young's modulus of endothelial cell	E_s	5 kPa	(6, 17)
Young's modulus of PMNs	E_0	5 kPa	(6, 17)
Clutch spring constant	K_C	1 nN·nm^{-1}	(13)
Viscosity constant	η	25 pN min ·µm^{-3}	(6, 7)
Total amount of traction force	F_M	20 nN	(11)
Threshold force	F_r	30 pN	(13, 32)
Cell radius	r_m	10 µm	This work
Compliance length	λ	0.1 nm	(12)
Mechanical feedback strength	$\delta\rho$	4	(13)
Total integrin number	N_{tot}	12000	This work
ICMA-I site density	L	200 µm^{-2}	This work
Protein radius	a	30 nm	(45)
Poisson's ratio	v_m	0.5	(45)

318

Downloaded from www.physiology.org/journal/ajpcell by ${individualUser.givenNames} ${individualUser.surname} (163.015.154.053) on August 28, 2018.
Copyright © 2018 American Physiological Society. All rights reserved.

319 **Results**

320

321 *Adhesion between hRBC-LSEC and hRBC-BMEC/bEnd.3 pairs is specifically*

322 *mediated by β_2-integrin-ICAM-1 interactions*

323 We first tested the expressions of ICAM-1 and β_2-integrin on distinct cells. ICAM-1

324 expression on intact or LPS- or TNF-α-stimulated LSECs, BMECs or bEnd.3 cells

325 and the site densities of coated LFA-1s or Mac-1s on hRBCs were determined using

326 flow cytometry (Fig. 1). ICAM-1 site density on LSECs was up-regulated from m_l =

327 232±41 to 388±78 μm^{-2} when cells were treated with 100 ng/ml TNF-α for 12 h, and

328 almost unchanged under 1 μg/ml LPS treatment for 12 h (m_l = 237±41 μm^{-2}) (Fig.

329 1A). This density was up-regulated distinctly from m_l = 733±89 to 1753±299 or

330 1182±129 μm^{-2} on BMECs (Fig. 1B), and enhanced equivalently from m_l = 69±18 to

331 215±39 or 211±41 μm^{-2} on bEnd.3 cells (Fig. 1C) under 1 μg/ml LPS or 100 ng/ml

332 TNF-α stimulation. Mouse LFA-1s or Mac-1s coated on hRBCs were determined for

333 each cell adhesion case, which all reads m_r = 12~92 μm^{-2} (Fig. 1D).

334

335 We next quantified the specific binding of an ICAM-1-expressed LSEC, BMEC or

336 bEnd.3 cell to a hRBC bearing LFA-1s or Mac-1s, using a steady-state adhesion

337 frequency by averaging the adhesion probabilities at sufficiently long contact duration

338 (t = 2 s for specific adhesion or t = 1 s for non-specific control). In the controls,

339 anti-ICAM-1 mAbs were pre-incubated with LSECs, MBECs or bEnd.3 cells before

340 tests. For each cell pair, the test cycle was repeated 80-100 times to obtain the running

341 frequency at a given duration (Fig. 2A). Adhesion between a LFA-1- or

Downloaded from www.physiology.org/journal/ajpcell by ${individualUser.givenNames} ${individualUser.surname} (163.015.154.053) on August 28, 2018.
Copyright © 2018 American Physiological Society. All rights reserved.

342 Mac-1-bearing hRBC and an ICAM-1-expressing LSEC was specific, since it yielded
343 high adhesion frequency value but was abolished when ICAM-1s were blocked (Fig.
344 2B-C). Moreover, the adhesion frequency was enhanced by TNF-α-stimulation to
345 LSECs. For bEnd.3 cells, no visible adhesion between the two cells was observed in
346 quiescent cells due to their quite low ICAM-1 expression (Fig. 1C). However, the
347 adhesion for LPS- or TNF-α-stimulated bEnd.3 cells was also specific, similar to
348 those observed for LSECs (Fig. 2F-G). Specifically, LFA-1-mediated adhesion
349 presented higher frequency in LPS-stimulation than that in TNF-α-stimulation while
350 Mac-1-mediated adhesion yielded same frequencies between the two stimuli.
351 Consistent with bEnd.3 cells, the adhesion frequencies for BMECs yielded higher
352 values under LPS stimulation than TNF-α stimulation, both of which can be abolished
353 when ICAM-1s were blocked (Fig. 2D-E). These results demonstrated that
354 hRBC-LSEC and hRBC-BMEC/bEnd.3 adhesion measured here was mediated by
355 specific β_2-integrin-ICAM-1 interactions.
356
357 *Binding of hepatic or cerebral ICAM-1s to β_2-integrins follows distinct kinetics.*
358 Specific adhesion frequency of a β_2-integrin-coated hRBC to a ICAM-1-expressing
359 LSEC, BMEC or bEnd.3 cell, P_a, was obtained by subtracting the ICAM-1-blocked
360 non-specific adhesion, P_n, from the total adhesion, P_t, using $P_a = (P_t - P_n)/(1 - P_n)$
361 with a given contact duration range of t = 0.25 - 5.0 s. The calculated P_a exhibited a
362 transition phase at short contact duration and then reached a plateau at sufficiently
363 long duration (Fig. 3). These data were fitted with the model using Eq. 1 (19, 43),
364 which read the correlation coefficient R^2 = 0.43-0.95 (Table 2). These fittings were

Downloaded from www.physiology.org/journal/ajpcell by ${individualUser.givenNames} ${individualUser.surname} (163.015.154.053) on August 28, 2018.
Copyright © 2018 American Physiological Society. All rights reserved.

365 seemingly reasonable when accounting for the potential diversity of those primary
366 endothelial cells. The paired kinetic parameters of the off-rate, k_r, and the cellular
367 binding affinity, $m_r m_l A_c K_a$, which were directly estimated from the prediction for the
368 binding curve, as well as the on-rate, $A_c k_f$, which was calculated from $A_c k_f = (m_r m_l A_c K_a) \times k_r / m_r m_l$,
369 were compared between Mac-1 and LFA-1 (Fig. 4). All the
370 parameters were then summarized in Table 2.

371

372 For quiescent LSECs, $m_r m_l A_c K_a$ was comparable for LFA-1 and Mac-1 (0.32 and 0.37,
373 respectively) but k_r for LFA-1 was 4.2-fold higher than that for Mac-1 (0.97 and 0.23
374 s^{-1}, respectively) (Fig. 4B). By excluding the contributions of different site densities of
375 the interacting molecules, the fitted parameters had a comparable effective affinity per
376 molecule ($A_c K_a = 2.19 \times 10^{-5}$ and 2.80×10^{-5} μm^4, respectively) (Fig. 4C) but a 3.3-fold
377 higher on-rate ($A_c k_f$ = 2.12×10^{-5} and 0.64×10^{-5} $\mu m^4 s^{-1}$, respectively) for LFA-1
378 compared with Mac-1 (Fig. 4A). These kinetic differences between LFA-1 and Mac-1
379 were confirmed when TNF-α was used to pre-treat LSECs to mimic inflammatory
380 responses in hepatic sinusoids. The equilibrium adhesion frequency was enhanced
381 from 0.28 and 0.17 in quiescent state to 0.44 and 0.54 in TNF-α stimulation for
382 LFA-1 and Mac-1, respectively (Fig. 3A-B). Evidently, the binding of Mac-1 to
383 LSEC-bearing ICAM-1 presented a relatively long period to reach the plateau (Fig.
384 3B), implying a slow kinetics of Mac-1 compared with LFA-1 (Fig. 3A). Fitted
385 parameters yielded a 1.8-fold higher on-rate, a 5.5-fold higher off-rate, but a 3.1-fold
386 lower binding affinity for LFA-1 compared to Mac-1 (Fig. 4A-C). For activated

Downloaded from www.physiology.org/journal/ajpcell by ${individualUser.givenNames} ${individualUser.surname} (163.015.154.053) on August 28, 2018.
Copyright © 2018 American Physiological Society. All rights reserved.

387 LSECs, these kinetic differences between the two integrins were reduced for the

388 on-rate but increased for both the off-rate and the effective affinity, indicating that

389 TNF-α stimulation narrows down the gap for association kinetics but expands the

390 difference for dissociation kinetics or binding capacity between LFA-1 and Mac-1.

391

392 For BMECs, the kinetic differences between LFA-1 and Mac-1 observed above were

393 confirmed when TNF-α or LPS was used to pre-treat BMECs. Intriguingly, the

394 equilibrium adhesion frequency was different in TNF-α (0.32 or 0.14) or LPS (0.41 or

395 0.13) stimulation for LFA-1 and Mac-1, respectively (Fig. 3C-D). The kinetic

396 parameters yielded a 3.2-fold higher on-rate (1.72×10^{-5} and 5.40×10^{-6} μm^4s^{-1}), a

397 1.2-fold lower off-rate (3.08 and 3.72 s^{-1}) but a 3.9-fold higher binding affinity

398 (5.60×10^{-6} and 1.43×10^{-6} μm^4) for LFA-1 and Mac-1 in LPS stimulation, respectively

399 (Fig. 4D-F). Moreover, these parameters presented a 1.2-fold higher on-rate

400 (4.90×10^{-6} and 4.10×10^{-6} μm^4s^{-1}), a 1.6-fold lower off-rate (1.53 and 2.45 s^{-1}) but a

401 1.9-fold higher binding affinity (3.22×10^{-6} and 1.66×10^{-6} μm^4) for LFA-1 compared to

402 Mac-1 in TNF-α stimulation (Fig. 4D-F).

403

404 The binding of LFA-1s and Mac-1s to ICAM-1s on LSECs or BMECs employ

405 different mechanisms. Specifically, the effective affinity of Mac-1 to ICAM-1 is

406 always higher than that of LFA-1 to ICAM-1 on LSECs but lower than that of LFA-1

407 to ICAM-1 on BMECs. To further confirm this difference, the ICAM-1s on bEnd.3

408 cells, a frequently used murine brain endothelial cell line, were also tested. Same to

Downloaded from www.physiology.org/journal/ajpcell by ${individualUser.givenNames} ${individualUser.surname} (163.015.154.053) on August 28, 2018.
Copyright © 2018 American Physiological Society. All rights reserved.

409 BMECs, ICAM-1 on bEnd.3 cells interacted with LFA-1 with higher effective binding
410 affinity than Mac-1, 1.7-fold higher (9.93×10^{-5} to 5.81×10^{-5} μm^4) in LPS stimulation
411 and a 3.7-fold higher (5.83×10^{-5} and 1.58×10^{-5} μm^4) in TNF-α stimulation. Under
412 LPS stimulation LFA-1 yielded a 1.4-fold higher on-rate (2.13×10^{-4} and 1.52×10^{-4}
413 $\mu m^4 s^{-1}$) and a 1.2-fold lower off-rate (2.15 and 2.62 s^{-1}) than Mac-1. Under TNF-α
414 stimulation, the parameters presented a 3.9-fold higher on-rate (1.37×10^{-4} and
415 3.55×10^{-5} $\mu m^4 s^{-1}$), a comparable off-rate (2.35 and 2.25 s^{-1}) (Fig. 4G-I).
416
417 Taken together, comparing the fitted mean values of kinetic parameters makes a sense
418 to illustrate the binding differences of LFA-1s and Mac-1s to ICAM-1s on varied
419 endothelial cells. These results indicated that ICAM-1s on hepatic sinusoidal
420 endothelial cells and cerebral microvascular endothelial cells present opposite binding
421 regulation in interacting with LFA-1 or Mac-1. These findings might be related to the
422 distinct tissue-specific PMN recruitment in liver and brain.
423
424 *PMN free crawling on LSEC, BMEC or bEnd.3 monolayer mediated by*
425 *β_2-integrin-ICAM-1 interactions*
426 To test the above hypothesis upon molecular binding kinetics, free crawling dynamics
427 of BM PMNs on TNF-α-stimulated LSEC, BMEC or bEnd.3 monolayer was
428 quantified (Fig. 5). Here PMNs presented high expression of both LFA-1s and Mac-1s,
429 as measured in Fig. 1D. LSECs, BMECs or bEnd.3 cells were stimulated by 100
430 ng/ml TNF-α for 12 h before tests and PMNs were pre-incubated with LFA-1 or

Downloaded from www.physiology.org/journal/ajpcell by ${individualUser.givenNames} ${individualUser.surname} (163.015.154.053) on August 28, 2018.
Copyright © 2018 American Physiological Society. All rights reserved.

431 Mac-1 blocking mAbs to isolate the respective role of Mac-1s or LFA-1s in PMN
432 crawling. On TNF-α-stimulated LSEC monolayer (Fig. 5A-C), 20% of intact PMNs
433 tended to crawl onto the monolayer. Blockage of either LFA-1 or Mac-1 reduced
434 slightly the crawling fraction without statistical differences (Fig. 5B). By contrast, the
435 mean crawling speed (~4.59 μm/min) for intact PMN was significantly reduced by
436 blocking Mac-1 (~3.74 μm/min), but not blocking LFA-1 (Fig. 5C). On
437 TNF-α-stimulated BMEC monolayer (Fig. 5D-F), the crawling fraction (~8%) and
438 speed (3.72 μm/min) for intact PMNs were lower to those on TNF-α-stimulated LSEC
439 monolayer, and the crawling speed was down-regulated by blocking LFA-1 (3.56
440 μm/min) (Fig. 5E-F). Again, LFA-1 or Mac-1 blockage had no effects on the crawling
441 fraction (Fig. 5E). On TNF-α-stimulated bEnd.3 monolayer (Fig. 5D-F), the crawling
442 fraction (~28%) and speed (4.76 μm/min) for intact PMNs were similar to those on
443 TNF-α-stimulated LSEC monolayer (Fig. 5H-I) and LFA-1 or Mac-1 blockage had no
444 effects on the crawling fraction (Fig. 5H). The crawling speed was lowered by
445 blocking LFA-1 (~3.85 μm/min), but not blocking Mac-1 (~4.46 μm/min) (Fig. 5I).
446 Although PMN crawling was not identical between cerebral microvascular BMEC
447 and bEnd.3 monolayers, both β_2 integrin members yielded similar mechanisms that
448 blocking LFA-1 reduced the crawling speed but blocking Mac-1 had no effect on
449 crawling dynamics, which is opposite to those on hepatic sinusoidal LSEC monolayer.
450 These data suggest that Mac-1 and LFA-1 play a dominant role in PMN crawling on
451 hepatic sinusoidal and cerebral microvascular endothelium, respectively.
452

Downloaded from www.physiology.org/journal/ajpcell by ${individualUser.givenNames} ${individualUser.surname} (163.015.154.053) on August 28, 2018.
Copyright © 2018 American Physiological Society. All rights reserved.

453 PMN free crawling on endothelium is mainly governed by their binding kinetics of
454 the interacting molecules. Considering that the site densities of LFA-1 and Mac-1 on
455 intact PMNs were equal (m_r^{LFA-1} = 22 μm^{-2}, m_r^{Mac-1} = 24 μm^{-2}) (Fig. 1D), this crawling
456 speed difference in LFA-1- or Mac-1-mediated PMN crawling on LSEC and
457 BMEC/bEnd.3 monolayer is presumably attributed to the distinct characteristics of the
458 tissue-specific β_2-integrin-ICAM-1 interactions. Noticing that the site density of
459 ICAM-1 expression was different on TNF-α-stimulated LSECs, BMECs and bEnd.3
460 cells (m_l^{LSEC} = 388 μm^{-2}, m_l^{BMEC} = 1182 μm^{-2}, $m_l^{bEnd.3}$ = 211 μm^{-2}) (Fig. 1A-C), this
461 difference does not affect the capacity of PMN adhering on endothelial cells. This is
462 because, upon 2D binding kinetics theory (9), the binding kinetics of
463 β_2-integrin-ICAM-1 pair is determined by the one molecular species with minimal site
464 density, *that is*, β_2-integrin (LFA-1 o Mac-1) in the current work. Thus, it is
465 reasonably speculated, upon the binding kinetics differences measured (Fig. 4), that
466 high effective affinity of β_2 integrin-ICAM-1 would lead to high crawling speed of
467 PMNs on tissue-specific endothelium but has no relevance with PMN crawling
468 fraction.
469
470 *Binding characteristics of hepatic or cerebral ICAM-1s to β_2-integrin are biologically*
471 *relevant with PMN free crawling*
472 In order to elucidate how the binding kinetics affects PMN free crawling, theoretical
473 predictions based on FEM and MCM were conducted to determine the contributions
474 of tissue-specific β_2-integrin-ICAM-1 kinetics to PMN crawling on endothelium.

Downloaded from www.physiology.org/journal/ajpcell by ${individualUser.givenNames} ${individualUser.surname} (163.015.154.053) on August 28, 2018.
Copyright © 2018 American Physiological Society. All rights reserved.

475 Briefly, the integrin-ligand bonds become stretched when a cell is moving. Those
476 bonds with smaller off-rate (k_r) sustain larger force before break-up, which initiates
477 the mechanical feedback loop and then leads to the increase of activated integrins (Fig.
478 6A-C). The number of bound integrins, which positively defines the level of active
479 force through connecting actin and myosin II components, is further determined by
480 on-rate (k_f), which is iterated by the time-lapsed local concentration of active integrins
481 (Fig. 6D-G). Supposing that the endothelium monolayer's rigidity is 5 kPa, the
482 increment of drag force by one integrin-ligand bond is relatively small compared with
483 that of active force (Fig. 7A-F). This net force increases with time and exhibits a
484 transition phase followed by an equilibrium state, suggesting that the cell crawling
485 speed is determined competitively by drag force and active force. Accordingly, the
486 integrin-ligand interactions with higher binding affinity mediate firm cell-cell
487 adhesion, and thus, higher cell motility.
488
489 From this model, PMN crawling speed was calculated based on the measured kinetics
490 parameters and the corresponding site densities on cell surfaces (Fig. 3, 4). Here an
491 ascending transition of PMN crawling is presented initially (0~4 min) before reaching
492 a plateau (Fig. 7G-I), which is in accordance with the predicted time courses of net
493 force (Fig. 7A-F). The plateau active and drag forces were also compared on
494 TNF-α-stimulated LSEC, BMEC or bEnd.3 cells, which reads the relatively higher
495 values for Mac-1-associated PMN crawling on LSECs and LFA-1-associated PMN
496 crawling on BMECs or bEnd.3 cells (Fig. 7J-L). Equilibrium crawling speed was

Downloaded from www.physiology.org/journal/ajpcell by ${individualUser.givenNames} ${individualUser.surname} (163.015.154.053) on August 28, 2018.
Copyright © 2018 American Physiological Society. All rights reserved.

497 further compared between LFA-1- and Mac-1-ICAM-1-mediated crawling on two
498 types of endothelial cells (Fig. 7M), indicating that PMN crawling speed on LSEC
499 monolayer is low on LFA-1-ICAM-1 mediation but high on Mac-1-ICAM-1
500 mediation while this speed dependence on β_2-integrin-ICAM-1 mediation is opposite
501 on BMEC or bEnd.3 monolayer (Fig. 7I), implying that these simulations are
502 consistent well with measured data (Fig. 5). In addition, the simulated crawling speed
503 on BMEC monolayer is lower but has the same regulation compared with that on
504 bEnd.3 monolayer, also in agreement with the experimental data. Taking both
505 experimental data and numerical simulations together (Fig. 5, 7), PMN crawling
506 speed is positively correlated to the effective binding affinity of β_2-integrin and
507 ICAM-1 pairs and Mac-1- or LFA-1-ICAM-1 interactions are dominant in PMN free
508 crawling on hepatic sinusoidal or cerebral microvascular endothelial cell monolayer.
509

Downloaded from www.physiology.org/journal/ajpcell by ${individualUser.givenNames} ${individualUser.surname} (163.015.154.053) on August 28, 2018.
Copyright © 2018 American Physiological Society. All rights reserved.

510 **Table 2. Summary of kinetic parameters of β_2-integrin and ICAM-1 bindings**
511 **between ECs and hRBCs.**

Data set	k_r^0, s^{-1}	$A_cK_a \times 10^5$, μm^4	$A_ck_f \times 10^5$, $\mu m^2 s^{-1}$	R^2
Unstimulated LSECs with LFA-1 coated hRBCs	0.97	2.19	2.12	0.48
Unstimulated LSECs with Mac-1 coated hRBCs	0.23	2.80	0.64	0.53
TNF-α-stimulated LSECs with LFA-1 coated hRBCs	2.62	3.00	7.88	0.69
TNF-α-stimulated LSECs with Mac-1 coated hRBCs	0.48	9.26	4.41	0.95
TNF-α-stimulated BMECs with LFA-1 coated hRBCs	1.53	0.32	0.49	0.90
TNF-α-stimulated BMECs with Mac-1 coated hRBCs	2.45	0.17	0.41	0.60
LPS-stimulated BMECs with LFA-1 coated hRBCs	3.08	0.56	1.72	0.71
LPS-stimulated BMECs with Mac-1 coated hRBCs	3.72	0.14	0.54	0.43
TNF-α-stimulated bEnd.3 cells with LFA-1 coated hRBCs	2.35	5.83	13.71	0.45
TNF-α-stimulated bEnd.3 cells with Mac-1 coated hRBCs	2.25	1.58	3.55	0.44
LPS-stimulated bEnd.3 cells with LFA-1 coated hRBCs	2.15	9.93	21.35	0.75
LPS-stimulated bEnd.3 cells with Mac-1 coated hRBCs	2.61	5.81	15.17	0.68

512

Downloaded from www.physiology.org/journal/ajpcell by ${individualUser.givenNames} ${individualUser.surname} (163.015.154.053) on August 28, 2018.
Copyright © 2018 American Physiological Society. All rights reserved.

513 ## Discussions

514

515 Binding of ICAM-1 ligands to β_2-integrin receptors is critical for supporting the
516 residence of flowing PMNs. Here we compared the binding kinetics of LFA-1- and
517 Mac-1-ICAM-1 pair, as well as their regulation in related PMN crawling, attempting
518 to elucidate the biophysical characteristics of β_2-integrin-ICAM-1 in mediating PMN
519 recruitment in liver and brain. Our data indicated that binding of hepatic or cerebral
520 ICAM-1 to β_2-integrin follows distinct kinetics. The effective affinity of Mac-1 to
521 ICAM-1 is always higher than that of LFA-1 on LSECs, while this pattern is reversed
522 for ICAM-1s expressed on BMECs or bEnd.3 cells. To our knowledge, this is the first
523 to quantify the distinct contributions of LFA-1 and Mac-1 in regulating PMN
524 adhesion and crawling specifically on hepatic sinusoidal and cerebral microvascular
525 endothelium. These exceptional findings come from the binding affinity between
526 ICAM-1-β_2-integrin pair for interacting LSECs and PMNs, where it is higher for
527 ICAM-1-Mac-1 binding than that for ICAM-1-LFA-1 binding. This is different from
528 previous measurements when soluble ICAM-1s are captured onto microbeads (26) or
529 when membrane-bound ICAM-1s are constitutively expressed on human pulmonary
530 microvascular endothelial cells or human WM9 metastatic melanoma cells (25, 26).

531

532 Binding kinetics of ICAM-1-β_2-integrin pair is critical when PMNs adhere to, migrate
533 along, and cross over the endothelium. These distinct kinetic features of hepatic and
534 cerebral ICAM-1s are physiologically relevant. The affinity differences in binding of

Downloaded from www.physiology.org/journal/ajpcell by ${individualUser.givenNames} ${individualUser.surname} (163.015.154.053) on August 28, 2018.
Copyright © 2018 American Physiological Society. All rights reserved.

535 ICAM-1s to Mac-1s and LFA-1s are consistent with PMN crawling speed on LSEC,
536 BMECs or bEnd.3 monolayer. Specifically, Mac-1-ICAM-1 interactions dominantly
537 affect PMN crawling on LSEC monolayer with its high affinity, while on BMEC or
538 bEnd.3 monolayer high affinity LFA-1-ICAM-1 interactions are crucial in PMN
539 crawling (Fig. 4, 5). These results provide a clue to correlate the molecular binding
540 kinetics and cellular crawling dynamics, at least, in the two aspects. First, it is known
541 that LFA-1 usually presents a fast kinetics and then functions within ~300 s but Mac-1
542 often yields a slow kinetics functioning from ~350 s when PMNs flow over the
543 endothelium in conventional microcirculation (27). This is supported from the
544 observed differences in transition phases between LFA-1 and Mac-1 in the current
545 work, where Mac-1 needs to take longer time to reach the plateau (Fig. 3). Second, the
546 adhesion and migration of flowing PMNs onto LSECs are quite specific *in vivo*,
547 where Mac-1 seems to play a dominant role, but not LFA-1 (30). By contrast, low
548 bindings of β_2-integrins (comparable affinity for LFA-1s but much lower value for
549 Mac-1s) on BMECs or bEnd.3 cells (Fig. 4) could contribute, at least partially, to the
550 difficulty for PMNs adhering on and transmigrating across BBB (18). Our data
551 indicate that these observations are presumably due to the binding features of
552 β_2-integrins either constitutively expressed or chemically coupled to ICAM-1 ligands
553 on tissue-specific distinct endothelium (Fig. 4). These results exemplify the
554 integration of molecular binding kinetics and cellular cell crawling dynamics.
555
556 Theoretical modeling is a potential approach to bridge the sophisticated molecular

Downloaded from www.physiology.org/journal/ajpcell by ${individualUser.givenNames} ${individualUser.surname} (163.015.154.053) on August 28, 2018.
Copyright © 2018 American Physiological Society. All rights reserved.

557 binding and cellular crawling when the evidences in intermediate signaling events
558 remain ultimately unclear. At molecular level, either a probabilistic or a deterministic
559 model of small system kinetics is well applied to quantify the receptor-ligand binding
560 kinetics from distinct viewpoints of the intrinsic features of interacting molecules (1, 9,
561 46). Meanwhile, the mechano-chemical coupling models propose the force
562 dependence of receptor-ligand bond dissociation (3, 9, 24). At cellular level, those cell
563 crawling models suggest that the randomized movement of a cell on substrate is
564 mainly attributed by actin polymerization at cell front for pushing cell moving
565 forward (3, 42), but few of them correlate cell movement with their basolateral
566 binding molecules on substrate. Here we integrate the basic models from both ends,
567 simply taking the cell moving at a static force balance and the receptor-ligand pair
568 bonding as a deterministic event. Intracellular signaling is not taken into account
569 explicitly, instead, simplified in terms of summed elastic stress of cytoskeletal actin
570 driven by various types of signaling molecules (14). Without loss of generality, our
571 simulations help to validate the above experimental observations on
572 β_2-integrin-ICAM-1 binding and PMN free crawling, and further the understanding in
573 the tissue-specificity of PMN recruitment to liver and brain. Noting that the force
574 applied on integrin-ligand bond dominates the signal reception process of
575 integrin-mediated mechanosensing and finally determines cell crawling speed (8, 29,
576 36, 42), future issues would be focused on elucidating the global picture of
577 integrin-mediated mechanosensing, since a body of molecular mechanisms, such as
578 molecular motor activity, integrin clustering, and focal adhesion remodeling, are

Downloaded from www.physiology.org/journal/ajpcell by ${individualUser.givenNames} ${individualUser.surname} (163.015.154.053) on August 28, 2018.
Copyright © 2018 American Physiological Society. All rights reserved.

579 involved in the process *in vivo.*

580

581 Comparison of current *in vitro* functional tests with those *in vivo* studies reported in
582 the literature (30, 42) also supported the finding that Mac-1s dominate PMN
583 recruitment to hepatic sinusoids by local chemokine or cytokine stimulation, while
584 LFA-1s play a key role in PMN recruitment to brain. Differential functions of LFA-1s
585 and Mac-1s present tissue-specific characteristics, at least, between liver and brain,
586 presumably due to their distinct anchoring features of ICAM-1 molecules onto
587 differential types of endothelial cells, *i.e.*, endothelial cell mechanics and ICAM-1
588 conformation (21), or their distinct chemokine/chemoattractant signals on LSEC,
589 BMEC or bEnd.3 cell surface to activate LFA-1 and Mac-1. More importantly, our
590 results first clarified these physiological processes using well-defined biophysical
591 approaches, which provide a mechanistic insight into relating binding kinetics of
592 hepatic sinusoidal and cerebral microvascular ICAM-1 to PMN crawling.

Downloaded from www.physiology.org/journal/ajpcell by ${individualUser.givenNames} ${individualUser.surname} (163.015.154.053) on August 28, 2018.
Copyright © 2018 American Physiological Society. All rights reserved.

593 ## Grant

594

595 This work was supported by National Natural Science Foundation of China grants
596 31230027, 91642203, and 31661143044, Chinese Academy of Sciences Strategic
597 Priority Research Program XDB22040101 and Frontier Science Key Project
598 QYZDJ-SSW-JSC018, and National Key Research and Development Program of
599 China grant 2016YFA0501601.

600

601 ## Disclosures

602

603 The authors declare no competing financial interests.

604

605 ## Author contributions

606

607 C.F.T., Y.Z., S.Q.L., and M.L. conceived and designed research; C.F.T., Y.X.G., H.Y.,
608 and Y.D. performed experiments; C.F.T., S.L.F., and D.D.H. analyzed data; C.F.T.,
609 Y.Z., S.Q.L., N.L., Y.X.G., H.Y., and M.L. interpreted results of experiments; C.F.T.
610 prepared figures; C.F.T., and M.L. drafted manuscript. C.F.T., Y.Z., S.Q.L., N.L.,
611 S.L.F., and M.L. edited and revised manuscript. C.F.T., Y.Z., S.Q.L., N.L., Y.X.G.,
612 H.Y., S.L.F., Y.D. D.D.H., and M.L. approved final version of manuscript.

Downloaded from www.physiology.org/journal/ajpcell by ${individualUser.givenNames} ${individualUser.surname} (163.015.154.053) on August 28, 2018.
Copyright © 2018 American Physiological Society. All rights reserved.

613 # Figures

614

615 **Figure 1. Expressions of murine ICAM-1 and β_2-integrin molecules.** ICAM-1s
616 constitutively expressed on mouse primary hepatic LSECs (**A**) and cerebral BMECs
617 (**B**) or immortalized cerebral bEnd.3 cells (C), or LFA-1s and Mac-1s constitutively
618 expressed on mouse PMNs (**D**) or coupled *via* chromium chloride on hRBCs (**E**),
619 were incubated with respective FITC-conjugated primary mAbs and analyzed by flow
620 cytometry (typical data from 3 to 12 independent experiments). PMNs, LSECs,
621 BMECs or bEnd.3 cells incubated with FITC-conjugated isotype-matched irrelevant
622 mAbs or plain hRBCs incubated with FITC-conjugated primary mAbs were used as
623 control. In some cases, LSECs, BMECs or bEnd.3 cells were pre-stimulated by 1
624 μg/ml LPS or by 100 ng/ml TNF-α for 12 h, respectively.

625

626 **Figure 2. Binding specificity.** (**A**) A test cycle of micropipette aspiration technique
627 (MAT) in four phases of approach, contact, withdrawal, and detachment. Here an
628 RBC (*dark cell*) serves as a force transducer to determine an adhesive event on
629 membrane deflection. Soluble LFA-1s or Mac1s were coated onto an RBC by $CrCl_3$
630 coupling while ICAM-1s were constitutively expressed on a mouse LSEC or BMEC
631 or bEnd.3 cell. Binding specificity was confirmed for RBC-LSEC pair in quiescent or
632 TNF-α-stimulated cases mediated by LFA-1- (**B**) or Mac-1-ICAM-1 (**C**) interactions
633 and for RBC-BMEC or RBC- bEnd.3 pair in LPS- or TNF-α-stimulated cases
634 mediated by LFA-1-(**D,F**) or Mac-1-ICAM-1 (**E,G**) interactions while non-specific
635 binding was tested by adding anti-ICAM-1 mAbs to the endothelial cells. The
636 adhesion frequency was obtained by averaging all the points at sufficient long contact
637 time (2 s for specific or 1 s for nonspecific binding). Data were presented as the mean
638 ± SEM. **, ****: P<0.01, 0.0001. *n* denotes the sample size.

639

640 **Figure 3. Binding curves of β_2-integrin-ICAM-1 interactions on LSECs, BMECs**
641 **or bEnd.3 cells.** Specific binding was quantified for ICAM-1s, expressed on LSECs

Downloaded from www.physiology.org/journal/ajpcell by ${individualUser.givenNames} ${individualUser.surname} (163.015.154.053) on August 28, 2018.
Copyright © 2018 American Physiological Society. All rights reserved.

642 (**A,B**) in quiescent Ca^{2+}/Mg^{2+} (*triangles*) or TNF-α-stimulated (*squares*) case, on
643 BMECs in TNF-α-stimulated (*squares*) or LPS-stimulated (*triangles*) case (**C,D**), or
644 on bEnd.3 cells in TNF-α-stimulated (*squares*) or LPS-stimulated (*triangles*) case
645 (**E,F**), to LFA-1- (**A,C,E**) or Mac-1-coupled (**B,D,F**) hRBCs. Non-specific binding
646 *via* blocking ICAM-1s on LSECs, BMECs or bEnd.3 cells was averaged for 3-5 cell
647 pairs at each contact duration (*not shown for clarity*) and then subtracted from total
648 adhesion at same duration. Data were presented as the mean ± SEM of adhesion
649 probability (*points*) for 3-5 independent experiment cell pairs. *Lines* were plotted
650 using the predictions fitted by Eq. 1.
651
652 **Figure 4. Kinetic parameters of β₂-integrin-ICAM-1 interactions on LSECs,**
653 **BMECs or bEnd.3 cells.** Effective on-rate A_ck_f (**A,D,G**), zero-force off-rate k_r
654 (**B**,**E,H**), and effective affinity A_cK_a (**C,F,I**) were compared for LSECs (**A-C**) in
655 Ca^{2+}/Mg^{2+} or TNF-α-stimulated cases, for BMECs (**D-F**) or bEnd.3 cells (**G-I**) in
656 TNF-α- or LPS-stimulated cases. The adhesion was mediated by LFA-1- (*white*
657 *bars*) or Mac-1-ICAM-1 (*black bars*) interactions in various cases. The parameters
658 were obtained by curve fitting the data sets in Fig. 3 (*points*; each set comes from 3-5
659 independent experiments) using Eq. 1.`
660
661 **Figure 5. PMN free crawling on LSEC, BMEC or bEnd.3 monolayer.** Typical
662 differential interference contrast images of crawling PMNs (*arrowheads*) onto a
663 LSEC (**A**), BMEC (**D**) or bEnd.3 (**G**) monolayer. Crawling fraction (**B,E,H**) and
664 speed (**C,F,I**) were plotted for intact (*white bars*), anti-LFA-1 mAb (*black bars*), and
665 anti-Mac-1 mAb (*grey bars*) -pre-incubated PMNs on TNF-α-stimulated LSEC (**B,C**),
666 BMEC (**E,F**) or bEnd.3 (**H,I**) monolayer during 30-60 min. Data are presented as the
667 mean ± SD from 3-7 frames and 30-200 cells in duplicate tests to calculate crawling
668 fraction and speed, respectively. [*], [****]: $P<0.05$, 0.001.
669
670 **Fig. 6. Theoretical modeling of PMN crawling onto endothelium.** (**A**) Finite
671 element model of cell lamellipod. The lamellipod is triangulated such that each node

Downloaded from www.physiology.org/journal/ajpcell by ${individualUser.givenNames} ${individualUser.surname} (163.015.154.053) on August 28, 2018.
Copyright © 2018 American Physiological Society. All rights reserved.

672 represents a mass of cytoskeleton contained in the surrounding (Voronoi) polygon.
673 Active forces are applied only at the front of the cell and exerted on the nodes marked
674 by *red dots*. (**B**) An element consists of a liner spring and a dashpot, accounting for
675 elastic effect and viscous dissipation associated with cytoskeleton-fluid friction,
676 respectively. (**C**) Bond formation and break up between integrins and ligands where
677 *red* and *black dots* denote the bound and unbound integrins, respectively. (**D-G**)
678 Time-lapsed snapshots of integrins activation modes at the time shortly after initiating
679 the simulation (t = 1 min) and at the moment of steady state (t = 12 min). Kinetic
680 parameters used in the simulations are adopted from experimental measurements of
681 Mac-1-ICAM-1 bindings for TNF-α-stimulated LSECs (*cf.* Fig. 4). The cell starts
682 with a circular shape initially. Color map indicates the normalized concentration of
683 activated integrins (**D**) and the number of bound integrins (**F**). At the steady state, the
684 cell reaches an elliptical shape (**E,G**). From the output of mechanical feedback, more
685 integrins are concentrated at the front of the cell (**E**), and more activated integrins
686 become associated with ICAM-1s locally (**G**), suggesting that the PMN-endothelium
687 adhesion is more firmly established at the front of the cell.
688
689 **Figure 7. Cellular active force, drag force and crawling speed predicted from the**
690 **calculations.** Time courses of active (*diamonds*) and drag (*cycles*) forces for PMN
691 crawling on TNF-α-stimulated LSEC (**A,D**), BMEC (**B,E**) or bEnd.3 (**C,F**)
692 monolayer mediated by LFA-1- (**A-C**) or Mac-1-ICAM-1 (**D-F**) interactions were
693 calculated using the measured kinetic parameters (*cf.* Fig. 4). The plateau values of
694 active (*white bars*) and drag (*gray bars*) forces were compared for TNF-α-stimulated
695 LSEC (**J**), BMEC (**K**) or bEnd.3 (**L**) cells. PMN crawling dynamics was also
696 predicted from the model using their kinetic parameters fitted from the data (*cf.* Fig. 4)
697 (**G-I**) and the estimated cell crawling speed was compared between LFA-1- (*white*
698 *bars*) and Mac-1-ICAM-1 (*black bars*) interactions (**M**). Data were presented as the
699 mean ± SEM. ****: P<0.0001. n denotes the sample size at the plateau in each case.
700

Downloaded from www.physiology.org/journal/ajpcell by ${individualUser.givenNames} ${individualUser.surname} (163.015.154.053) on August 28, 2018.
Copyright © 2018 American Physiological Society. All rights reserved.

701 # References:

702

703 1. **Bell GI**. Models for the specific adhesion of cells to cells. *Science* 200: 618-627, 1978.

704 2. **Bernardes M, Anthony DC, Issekutz AC, Perry VH**. Recruitment of neutrophils across the
705 blood–brain barrier: the role of E- and P-selectins. *J Cereb Blood Flow Metab* 21:1115–1124,
706 2001.

707 3. **Besser A, Schwarz US.** Coupling biochemistry and mechanics in cell adhesion: a model for
708 inhomogeneous stress fiber contraction. *New J Phys* 9: 425-425, 2007.

709 4. **Bieghs V, Trautwein C**. The innate immune response during liver inflammation and metabolic
710 disease. *Trends Immunol* 34: 446-452, 2013.

711 5. **Booth R, Kim H**. Characterization of a microfluidic in vitro model of the blood-brain barrier
712 (mBBB). *Lab Chip* 12: 1784-1792, 2012.

713 6. **Borau C, Kamm RD, García-Aznar JM**. Mechano-sensing and cell migration: a 3D model
714 approach. *Phys Biol* 8: 1347-1371, 2011.

715 7. **Bottino D, Mogilner A, Roberts T**, Stewart, M., & Oster, T. How nematode sperm crawl. *J*
716 *Cell Sci* 115: 367-384, 2012.

717 8. **Carlier MF, Pernier J, Montaville P, Shekhar S, Kühn S, Cytoskeleton Dynamics and**
718 **Motility group.** Control of polarized assembly of actin filaments in cell motility. *Cell Mol Life Sci*
719 72: 3051–3067, 2015.

720 9. **Chesla SE, Selvaraj P, Zhu C**. Measuring two-dimensional receptor-ligand binding kinetics by
721 micropipette. *Biophys J* 75: 1553-1572, 1998.

722 10. **Dixt N, Kim MH, Rossaint J, Yamayoshi I, Zarbock A, Simon SI**. Leukocyte function antigen-1,
723 kindlin-3, and calcium flux orchestrate neutrophil recruitment during inflammation. *J Immunol* 189:
724 5954-5964, 2012.

725 11. **Dokukina IV, Gracheva ME**. A model of fibroblast motility on substrates with different
726 rigidities. *Biophys J* 98: 2794-2803, 2010.

727 12. **Dong K, Dai JL**. Stabilizing to disruptive transition of focal adhesion response to mechanical
728 forces. *J Biomech* 43: 2524-2529, 2010.

729 13. **Elosegui-Artola A, Bazellières E, Allen MD, Andreu I, Oria R, Sunyer R, Gomm JJ,**

Downloaded from www.physiology.org/journal/ajpcell by ${individualUser.givenNames} ${individualUser.surname} (163.015.154.053) on August 28, 2018.
Copyright © 2018 American Physiological Society. All rights reserved.

730 **Marshall JF, Jones JL, Trepat X, Roca-Cusachs P**. Rigidity sensing and adaptation through
731 regulation of integrin types. *Na Mater* 13: 631-637, 2014.
732 14. **Floch'h AL, Huse M**. Molecular mechanisms and functional implications of polarized actin
733 remodeling at the T cell immunological synapse. *Cell Mol Life Sci* 72: 537–556, 2015.
734 15. **Fu CL, Tong CF, Dong C, Long M**. Modeling of cell aggregation dynamics governed by
735 receptor-ligand binding under shear flow. *Cell Mole Bioeng* 4**:** 427-441, 2011.
736 16. **Fu CL, Tong CF, Wang ML, Gao Y, Zhang Y, Lü SQ, Liang SL, Dong C, Long M**.
737 Determining beta2-integrin and intercellular adhesion molecule 1 binding kinetics in tumor cell
738 adhesion to leukocytes and endothelial cells by a gas-driven micropipette assay. *J Biol Chem* 286:
739 34777-34787, 2011.
740 17. **Ghibaudo M, Saez A, Trichet L, Xayaphoummine A, Browaeys J, Silberzan P, Buguin A,**
741 **Ladoux B**. Traction forces and rigidity sensing regulate cell functions. *Soft Matter* 4:
742 1836-1843, 2008.
743 18. **Gorina R, Lyck R, Vestweber D, Engelhardt B**. Beta(2) integrin-mediated crawling on
744 endothelial ICAM-1 and ICAM-2 is a prerequisite for transcellular neutrophil diapedesis across the
745 inflamed blood-brain barrier. *J Immunol* 192: 324-337, 2014.
746 19. **Huang J, Chen J, Chesla SE, Yago T, Mehta P, McEver RP, Zhu C, Long M**. Quantifying the
747 effects of molecular orientation and length on two-dimensional receptor-ligand binding kinetics. *J*
748 *Biol Chem* 279: 44915-44923, 2004.
749 20. **Jia XL, Chen J, Long M**. IL-8-induced L-selectin shedding regulates its binding kinetics to
750 PSGL-1. *Chinese Sci Bull* 54: 786-2793, 2009.
751 21. **Ji BH, Bao G**. Cell and molecular biomechanics: perspectives and challenges. *Acta Mech Solida*
752 *Sin* 24: 27-51, 2011.
753 22. **Kofler R, Wick G**. Some methodologic aspects of the chromium chloride method for coupling
754 antigen to erythrocytes. *J Immunol Methods* 16: 201-209, 1977.
755 23. **Kolaczkowska E, Kubes P**. Neutrophil recruitment and function in health and inflammation. *Nat*
756 *Rev Immunol* 13: 159-175, 2013.
757 24. **Kolsch V, Charest PG, Firtel, R. A**. The regulation of cell motility and chemotaxis by
758 phospholipid signaling. *J Cell Sci* 121: 551-559, 2008.
759 25. **Liang SL, Fu CL, Wagner D, Guo HG, Zhan DY, Dong C, Long M.** Two-dimensional kinetics

Downloaded from www.physiology.org/journal/ajpcell by ${individualUser.givenNames} ${individualUser.surname} (163.015.154.053) on August 28, 2018.
Copyright © 2018 American Physiological Society. All rights reserved.

760 of β_2-integrin and ICAM-1 bindings between neutrophils and melanoma cells in a shear flow. *Am.*
761 *J. Physiol Cell Physiol* 294: C743–C753, 2008.
762 26. **Li N, Mao D, Lü S, Tong C, Zhang Y, Long M.** Distinct binding affinities of Mac-1 and LFA-1
763 in neutrophil activation. *J Immunol* 190: 4371-4381, 2013.
764 27. **Lomakina EB, Waugh RE.** Signaling and dynamics of activation of LFA-1 and Mac-1 by
765 immobilized IL-8. *Cell Mole Bioeng* 3: 106-116, 2010.
766 28. **Long M, Zhao H, Huang KS, Zhu C**. Kinetic measurements of cell surface
767 E-selectin/carbohydrate ligand interactions. *Ann Biomed Eng* 29: 935-946, 2001.
768 29. **Maiuri P, Rupprecht JF, Wieser S, Ruprecht V, Bénichou O, Carpi N, Coppey M, De Beco S,**
769 **Gov N, Heisenberg CP, Lage Crespo C, Lautenschlaeger F, Le Berre M, Lennon-Dumenil**
770 **AM, Raab M, Thiam HR, Piel M, Sixt M, Voituriez R**. Actin flows mediate a universal coupling
771 between cell speed and cell persistence. *Cell* 161: 374–386, 2015.
772 30. **Menezes GB, Lee WY, Zhou H, Waterhouse CCM, Cara DC, Kubes P**. Selective
773 down-regulation of neutrophil Mac-1 in endotoxemic hepatic microcirculation via IL-10. *J*
774 *Immunol* 183: 7557-7568, 2009.
775 31. **Paschos KA, Canovas D, Bird NC.** The role of cell adhesion molecules in the progression of
776 colorectal cancer and the development of liver metastasis. *Cell Signal* 21: 665-674, 2009.
777 32. **Pere RC, Thomas I, Sheetz MP**. Finding the weakest link: exploring integrin-mediated
778 mechanical molecular pathways. *J Cell Sci* 125: 3025-3038, 2012.
779 33. **Petri B, Phillipson M, Kubes P**. The physiology of leukocyte recruitment: an in vivo perspective.
780 *J Immunol* 180: 6439-6446, 2008.
781 34. **Ramaiah SK, Jaeschke H**. Role of neutrophils in the pathogenesis of acute inflammatory liver
782 injury. *Exp Toxicol Pathol* 35: 757-766, 2007.
783 35. **Ruck T, Bittner S, Epping L, Herrmann AM, Meuth SG**. Isolation of primary murine brain
784 microvascular endotheliual cells. *J Vis Exp* 93: e52204, 2014.
785 36. **Scales TM, Parsons M**. Spatial and temporal regulation of integrin signalling during cell
786 migration. *Curr Opin Cell Biol* 23: 562-568, 2011.
787 37. **Selvaraj P, Plunkett ML, Dustin M, Sanders ME, Shaw S, Springer TA**. The T lymphocyte
788 glycoprotein CD2 binds the cell surface ligand LFA-3. *Nature* 326: 400-403, 1987.
789 38. **Shetty S, Weston CJ, Adams DH, Lalor PF**. A flow adhesion assay to study leucocyte

Downloaded from www.physiology.org/journal/ajpcell by ${individualUser.givenNames} ${individualUser.surname} (163.015.154.053) on August 28, 2018.
Copyright © 2018 American Physiological Society. All rights reserved.

790 recruitment to human hepatic sinusoidal endothelium under conditions of shear stress. *J Vis Exp* 21:
791 e51330, 2014.
792 39. **Shi D, Sun L, Mi G Sheikh L, Bhattacharya S, Nayar S, Webster TJ**. Controlling ferrofluid
793 permeability across the blood–brain barrier model. *Nanotechnology* 25: 075101-075101, 2014.
794 40. **Simon SI, Green CE**. Molecular mechanics and dynamics of leukocyte recruitment during
795 inflammation. *Annu Rev Biomed Eng* 7: 151-185, 2005.
796 41. **Spicer JD, McDonald B, Cools-Lartigue JJ, Chow SC, Giannias B, Kubes P, Ferri LE**.
797 Neutrophils promote liver metastasis via Mac-1-mediated interactions with circulating tumor cells.
798 *Cancer Res* 72: 3919-3927, 2012.
799 42. **Truebestein L, Elsner DJ, Fuchs, E, Leonard TA**. A molecular ruler regulates cytoskeletal
800 remodelling by the Rho kinases. *Nat Commun* 6: 10029-10029, 2015.
801 43. **Wu L, Xiao B, Jia X, Zhang Y, Lü S, Chen J, Long M**. Impact of carrier stiffness and
802 microtopology on two-dimensional kinetics of P-selectin and P-selectin glycoprotein ligand-1
803 (PSGL-1) interactions. *J Biol Chem* 282: 9846-9854, 2007.
804 44. **Xiao B, Tong C, Jia X, Guo R, Lü S, Zhang Y, McEver RP, Zhu C, Long M**. Tyrosine
805 replacement of PSGL-1 reduces association kinetics with P- and L-selectin on the cell membrane.
806 *Biophys J* 103: 777-785, 2012.
807 45. **Zhong Y, Ji B**. How do cells produce and regulate the driving force in the process of
808 migration. *Eur Phys J Special Topics* 223: 1373-1390, 2014.
809 46. **Zhu C, Bao G, Wang N**. Cell mechanics: mechanical response, cell adhesion, and molecular
810 deformation. measurements of cell surface E-selectin/carbohydrate ligand interactions. *Annu Rev*
811 *Biomed Eng* 2: 189-226, 2000.

Downloaded from www.physiology.org/journal/ajpcell by ${individualUser.givenNames} ${individualUser.surname} (163.015.154.053) on August 28, 2018.
Copyright © 2018 American Physiological Society. All rights reserved.

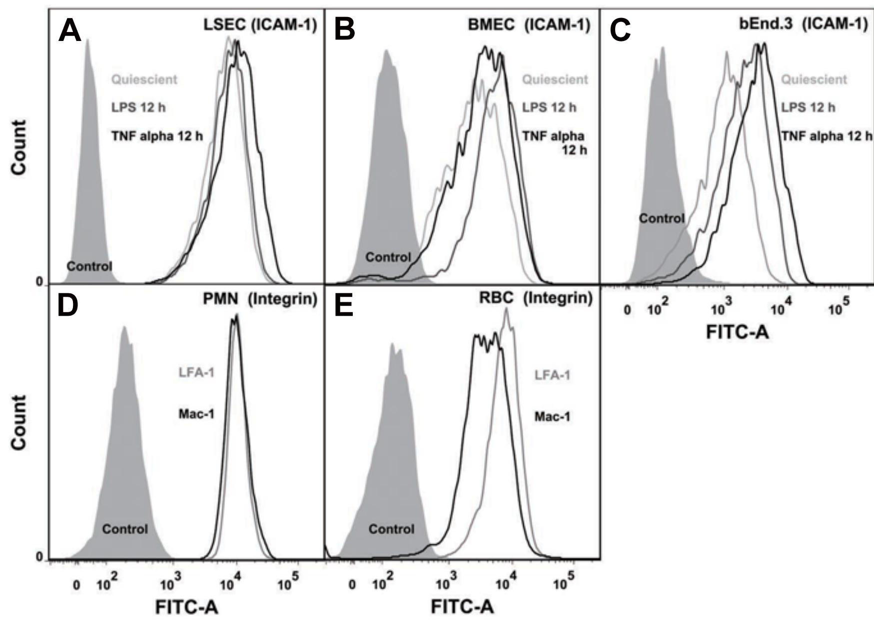

Downloaded from www.physiology.org/journal/ajpcell by ${individualUser.givenNames} ${individualUser.surname} (163.015.154.053) on August 28, 2018.
Copyright © 2018 American Physiological Society. All rights reserved.

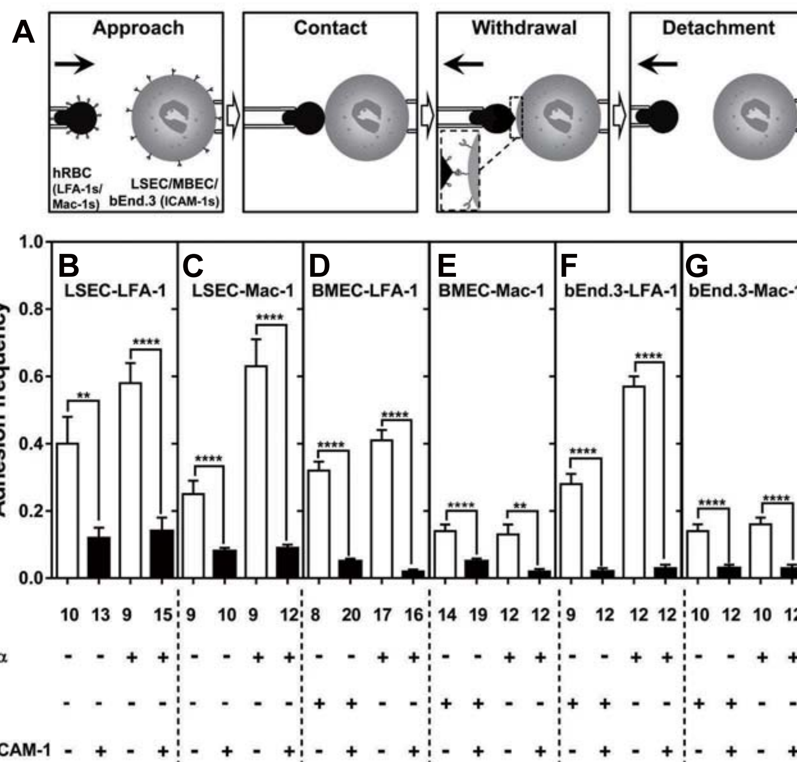

Downloaded from www.physiology.org/journal/ajpcell by ${individualUser.givenNames} ${individualUser.surname} (163.015.154.053) on August 28, 2018.
Copyright © 2018 American Physiological Society. All rights reserved.

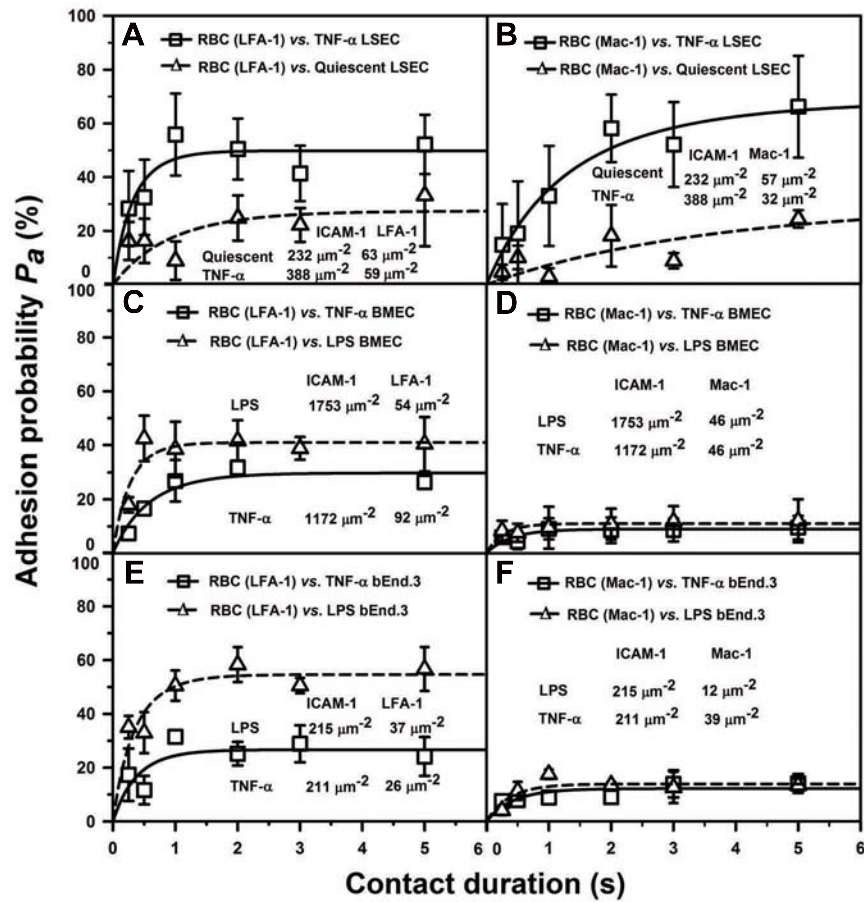

Downloaded from www.physiology.org/journal/ajpcell by ${individualUser.givenNames} ${individualUser.surname} (163.015.154.053) on August 28, 2018.
Copyright © 2018 American Physiological Society. All rights reserved.

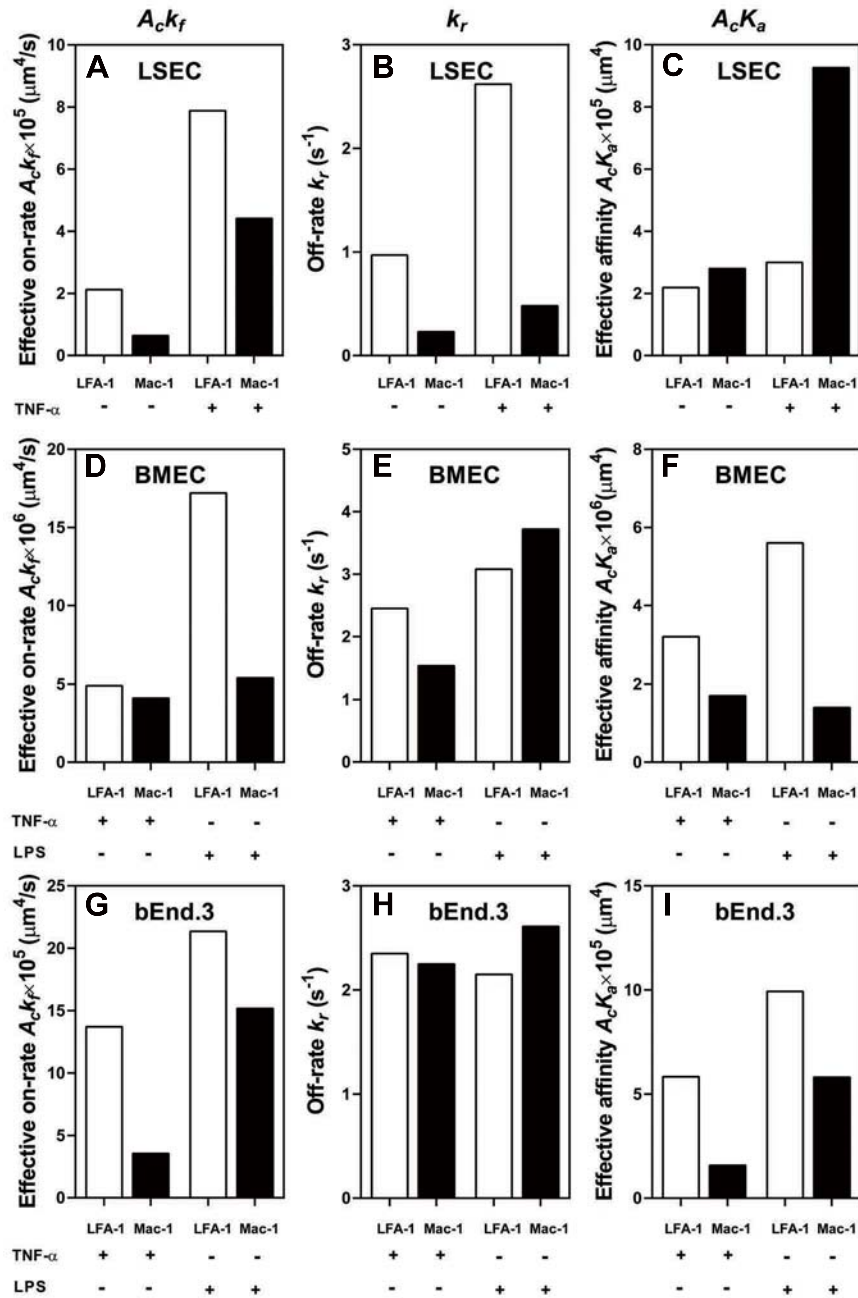

Downloaded from www.physiology.org/journal/ajpcell by ${individualUser.givenNames} ${individualUser.surname} (163.015.154.053) on August 28, 2018.
Copyright © 2018 American Physiological Society. All rights reserved.

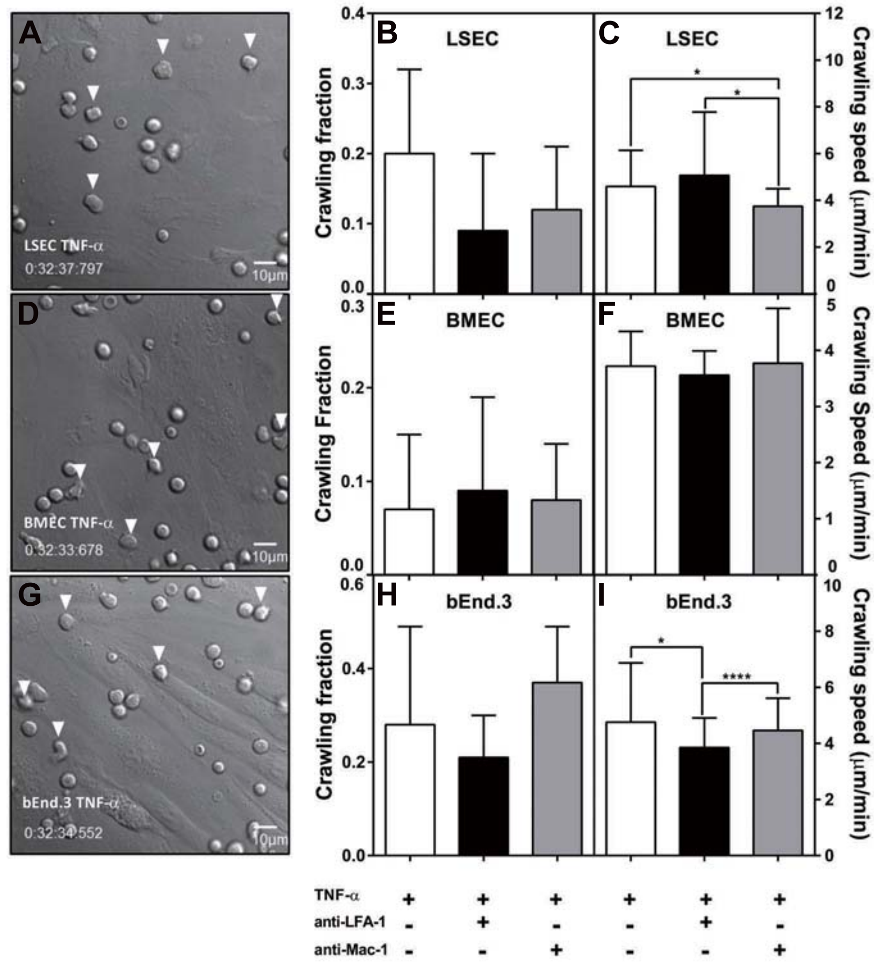

Downloaded from www.physiology.org/journal/ajpcell by ${individualUser.givenNames} ${individualUser.surname} (163.015.154.053) on August 28, 2018.
Copyright © 2018 American Physiological Society. All rights reserved.

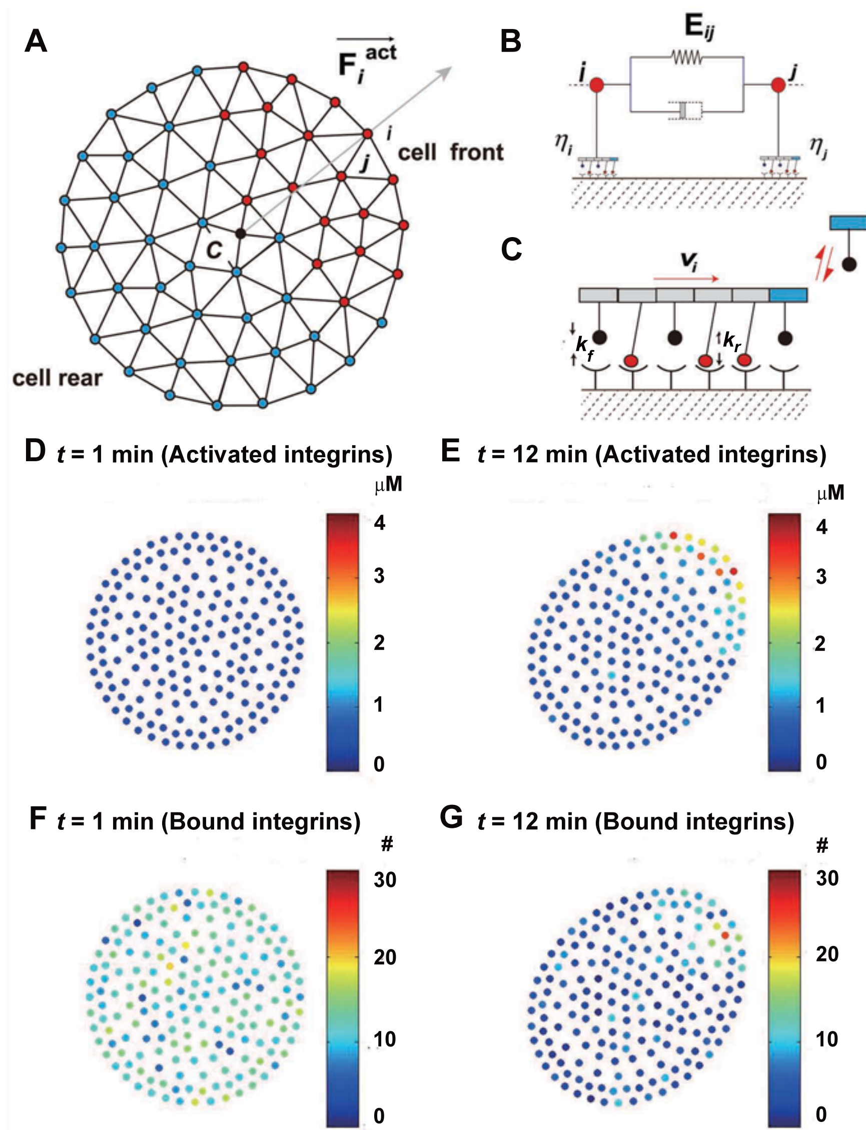

Downloaded from www.physiology.org/journal/ajpcell by ${individualUser.givenNames} ${individualUser.surname} (163.015.154.053) on August 28, 2018.
Copyright © 2018 American Physiological Society. All rights reserved.

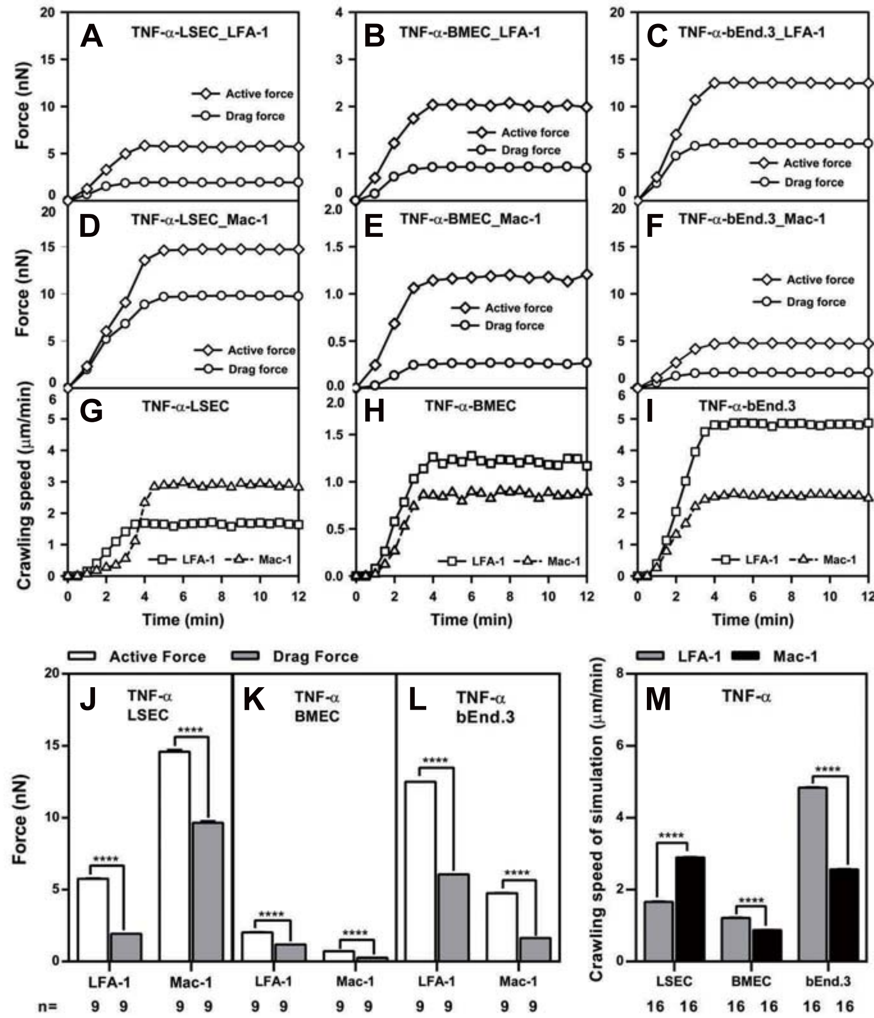

Downloaded from www.physiology.org/journal/ajpcell by ${individualUser.givenNames} ${individualUser.surname} (163.015.154.053) on August 28, 2018.
Copyright © 2018 American Physiological Society. All rights reserved.